Vol. B13 (1982) ACTA PHYSICA POLONICA No 10–11

HIGH-p_T HADRON-HADRON INTERACTIONS AND QCD*

By W. J. Metzger

Fysisch Laboratorium, University of Nijmegen**

(Received March 5, 1982)

Experimental results on hadroproduction of high-p_T particles is reviewed in the context of QCD.

PACS numbers: 11.10.Np, 13.85.-t

1. Introduction

In the parton picture, which grew out of deep inelastic electroproduction experiments in the late 1960s, a nucleon consists of three valence quarks and a sea of quark-antiquark pairs, a meson of a valence quark, a valence antiquark and a sea. With the advent of QCD a cloud of glouns was added to the constituents of hadrons. In parton models certain classes of hadron-hadron scattering factorize into an interaction between two of the constituents, carrying significant fractions of the incident hadron momentum, and an interaction between the remaining "spectator" partons. In this picture a hadron beam is regarded as a wide--band, unseparated parton beam (wide-band because the partons have a wide range of momentum and unseparated because all types of partons exist in the beam).

The best-studied situation is hadroproduction of lepton pairs. In the parton model the reaction proceeds through $q\bar{q}$ annihilation as proposed by Drell and Yan [1] which is shown in Fig. 1a. The factorization is ensured by the mediation of the virtual photon. In perturbative QCD the diagram of Fig. 1a is the lowest order diagram. This so-called Drell-Yan process provides an excellent testing ground for QCD. It will not be reviewed here[1] since there exist excellent recent reviews [2].

Factorization is also expected to occur in the production of large-p_T hadrons [3] pictured schematically in Fig. 1b. The interaction is then described by the structure functions

---

* Presented at the VI Autumn School of Theoretical Physics, Szczyrk, Poland, September 21–29, 1981, organized by the Silesian University, Katowice.

** Address: University of Nijmegen, Physics Department, Toernooiveld, 6525 ED Nijmegen, The Netherlands.

[1] This was reviewed in my first lecture at the VIth School.

of the colliding hadrons, the scattering matrix for the binary parton interaction and fragmentation functions for the scattered partons and for the spectator partons. The hard binary scattering is thought to take place over a much shorter time scale than the fragmen-

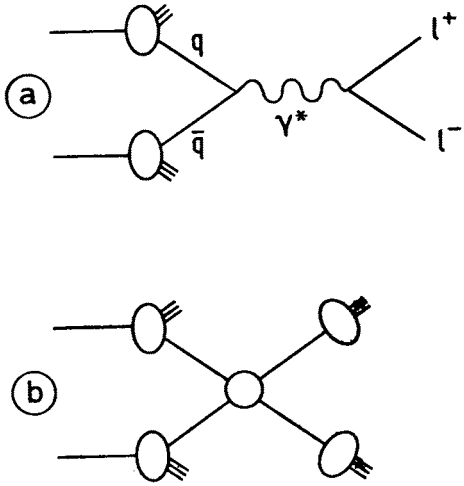

Fig. 1. (a) The Drell-Yan diagram; (b) High-p_T hadron production

tation, resulting in the factorization. An outgoing parton in Fig. 1b can be replaced by a photon, in which case there is of course no fragmentation. It is this case which will be reviewed in Section 2. In Section 3 the case of high-p_T hadrons will be examined.

2. Hadroproduction of high-p_T prompt photons

2.1. Introduction

In the last few years the subject of high-p_T photon production in hadron-hadron interactions has attracted a large amount of interest, both theoretical and experimental.

Theoretically single, prompt, high-p_T photons are expected to be produced in a hard scattering of two incident partons, the remaining partons in the incident hadrons playing only a spectator role (Fig. 2a). Such reactions are of particular interest because the lowest order QCD diagrams (Figs. 2b and 2c) all involve gluons. Note that these are the same diagrams which make up the first-order QCD corrections to Drell-Yan. Experimental evidence of these processes thus provides support for QCD (as opposed simply to a parton model which does not include gluons).

The study of these processes is experimentally quite difficult. There are several competing sources of single photons: Brehmsstrahlung from an outgoing quark, for example in a $qq \to qq$ subprocess (Fig. 2d); photon decay modes from mesons (e.g. $\eta, \omega, \ldots$); the conversion of a virtual vector meson to a real photon. In addition there are purely experimental problems with γ-pairs from π^0 and η decays: The two photons may be spatially

too close together to be resolved by the detector (the minimum angular separation of the two photons from π^0 decay is only $16^0/p$ in GeV); or the decay may be very asymmetric causing one of the photons to miss the detector completely. The requirement is thus for a detector of fine spatial resolution and large acceptance, which is expensive. Lacking

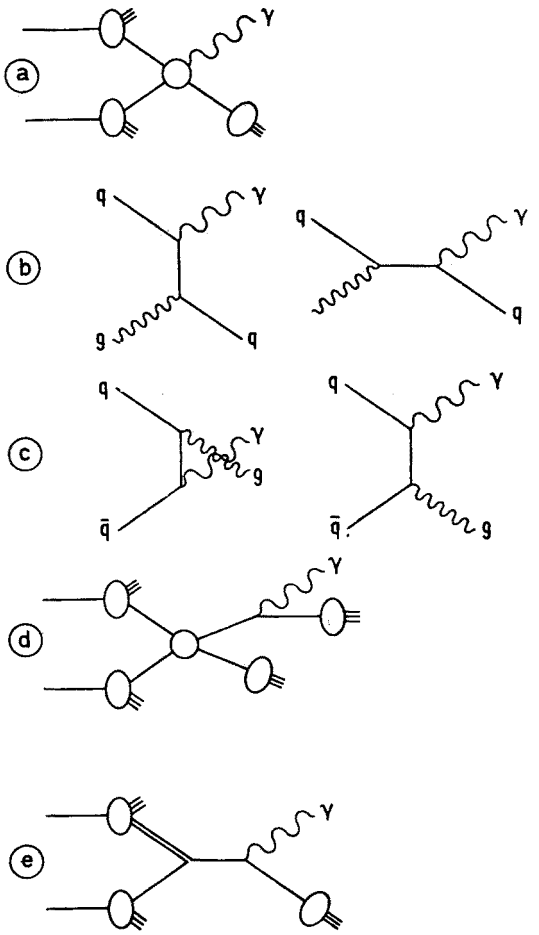

Fig. 2. (a) A hard scattering producing a prompt photon; (b) and (c) the lowest order QCD diagrams for prompt photon production; (d) production of a high-p_T photon by quark brehmsstrahlung; (e) a higher twist diagram which produces an unaccompanied prompt photon

fine enough granularity it is possible to separate the single photon signal statistically using the fact that the first photon conversion of a pair will on the average occur earlier in the detector than that of a single photon.

In all of the above sources of background the photon should be accompanied by hadrons, the other particles of the high-p_T jet. Other processes such as higher twists (Fig. 2e) could also lead to unaccompanied photons.

2.2. Cross sections

Early results [3] suggested the existence of prompt photons but were not conclusive having signals of less than 2 1/2 standard deviations. The more recent results of the AABC collaboration [4] on the ratio of photon to π^0 productions as function of p_T are shown

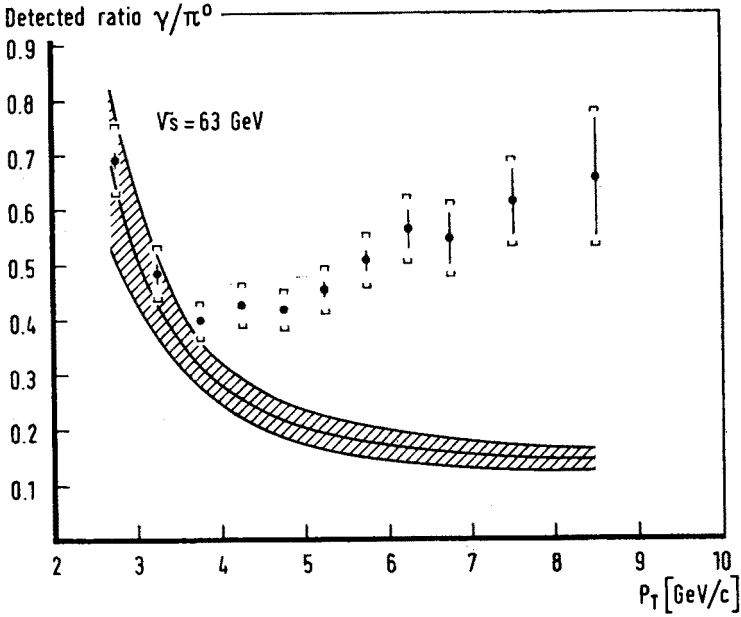

Fig. 3. The γ/π^0 ratio observed in p–p collisions at $\sqrt{s} = 63$ GeV. The curve represents a Monte Carlo calculation of the ratio assuming no direct photon production [4]

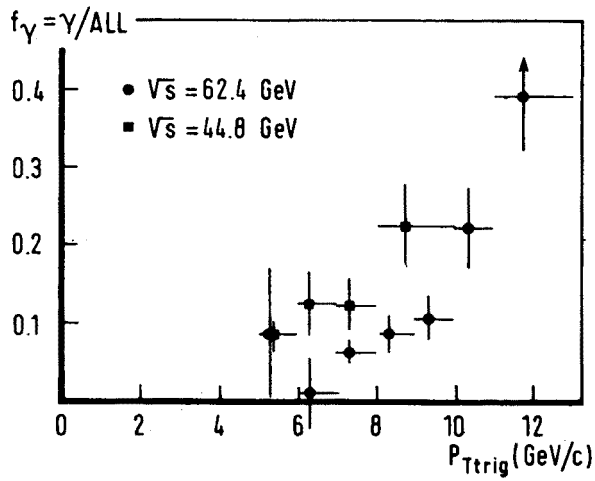

Fig. 4. The fraction of events attributed to direct-photon production as a function of $p_{T\,\mathrm{trigger}}$ in p–p collisions at $\sqrt{s} = 62.4$ and 44.8 GeV. The errors are statistical; there is in addition a systematic error of 5% [5]

in Fig. 3 together with a Monte Carlo background simulation. A prompt photon signal becomes apparent around $p_T \approx 4$ GeV/c and increases with p_T. The CCOR collaboration [5] using a statistical separation technique (and thus able to go to higher p_T) finds that the prompt-photon signal continues to increase with p_T as shown in Fig. 4 where the fraction of events attributed to prompt photon production is plotted. A Fermilab experiment has also observed the γ to π^0 ratio to increase with p_T [6].

Uncertainties in calculating $\sigma(\pi^0)$ or in the measured $\sigma(\pi^0)$ at high p_T and uncertainties in $\sigma(\gamma)$ from other sources ($\eta \to \gamma$, etc.) combined with uncertainties in the structure functions (in particular, f_g^p is almost unknown) resulted in very different calculations of $R(\gamma/\pi^0)$.

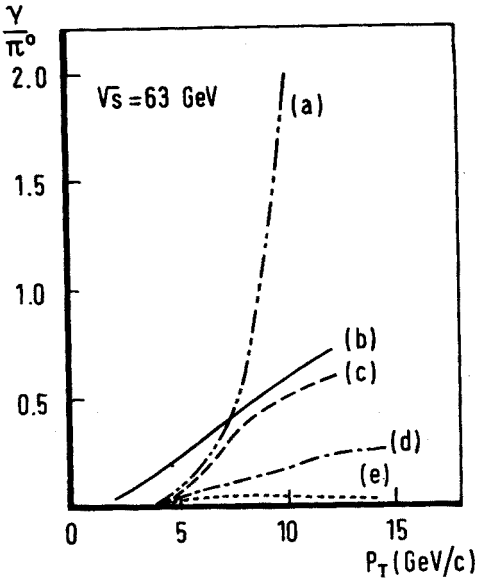

Fig. 5. Calculations of the γ/π^0 ratio for pp collisions at $\sqrt{s} = 63$ GeV from (a) Ref. [7], (b) Ref. [8], (c) Ref. [9], and (d), (e) Ref. [10]. The difference between curves (d) and (e) is the gluon structure function used: $g(x) \sim (1-x)^4$ in (d) and $g(x) \sim (1-x)^5$ in (e)

The situation just two years ago [7–10] is illustrated in Fig. 5. The appearance of experimental data resulted in a convergence of the calculations and rather good agreement with the data: Fig. 6 shows the background-subtracted AABC data on $R(\gamma/\pi^0)$ compared with curves calculated by Contogouris et al. [11]. Inclusion of soft gluon corrections (solid lines) improves the agreement compared to curves calculated without these corrections. Figure 7 shows the same data but now expressed as cross sections; the data and the different calculations are in fair agreement [12]. The soft gluon corrections will improve the agreement. The $\sqrt{s} = 63$ GeV data and the calculation of Halzen et al., are repeated in Fig. 8 where the $q\bar{q}$ and qg contributions are shown separately. It is seen that the qg subprocess dominates. This is due to the absence of valence antiquarks in p–p collisions.

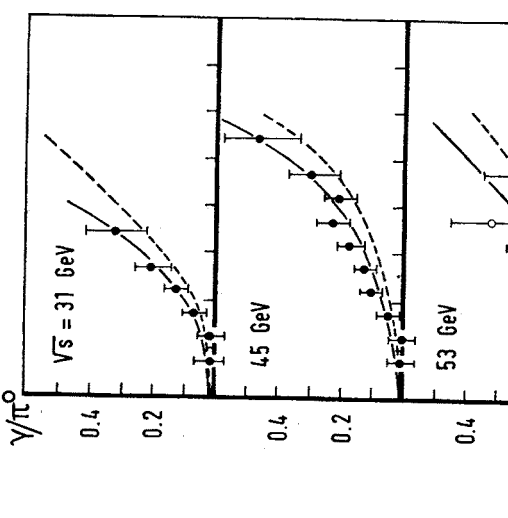

Fig. 6

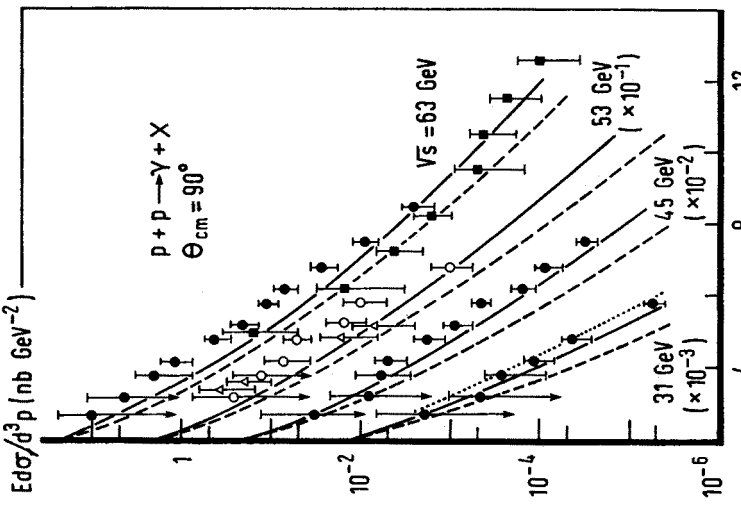

Fig. 7

Fig. 6. The background-subtracted γ/π^0 ratio in p–p collisions. The curves are calculated with (solid) and without (dashed) soft gluon corrections using a gluon structure function $g(x) \sim (1+9x)(1-x)^4$ [11]

Fig. 7. The invariant cross section for direct photon production in p–p collisions vs. the transverse momentum of the photon is compared to calculations by Contogouris et al. with $g(x) \sim (1-x)^4$ (solid line) and $g(x) \sim (1+9x)(1-x)^5$ (dashed line), by Halzen et al. (dashed-dot line), and by Owens et al. (dotted line). Except for $\sqrt{s} = 31$ GeV, the calculations of Owens et al. coincide with the solid lines. The figure is taken from Ref. [12]

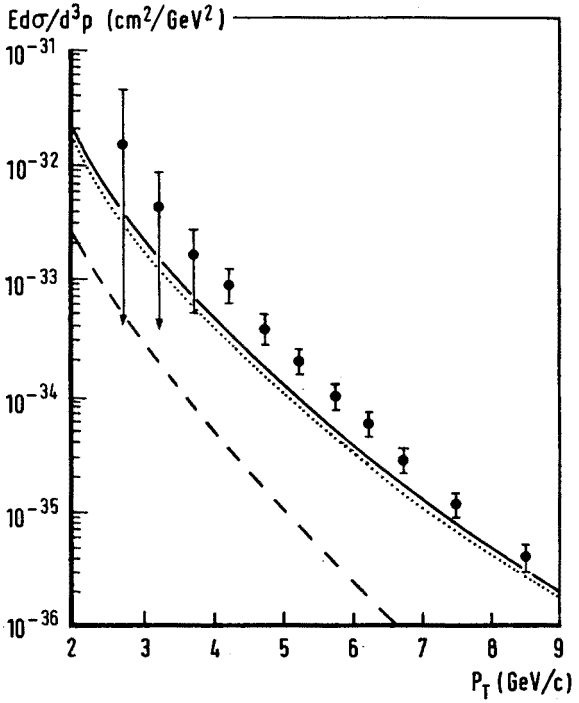

Fig. 8. The direct photon cross section at $y = 0$ vs. p_T for p–p collisions at $\sqrt{s} = 63$ GeV compared with the calculation of Halzen et al. [13] (solid line). The contributions of $gq \to \gamma q$ (dotted line) and $q\bar{q} \to \gamma g$ (dashed line) are shown separately. The gluon structure function was chosen as $g(x) = 3(1-x)^5$

2.3. Correlations

The QCD processes (Figs. 2b and 2c) should produce photons unaccompanied by hadrons. To investigate this the AABC collaboration [14] looked at rapidity correlations of same-side hadrons (charged particles and π^0's) with a π^0 trigger and with a γ trigger. The distribution of rapidity difference between the trigger particle and same-side charged particles is shown in Figs. 9a and 9b, respectively. The curves are a Monte Carlo estimate assuming uncorrelated particles. A large excess of particles is seen at small Δy in the π^0-trigger case; a smaller excess in the γ-trigger sample. Monte Carlo simulation of known sources of background (coalesced photons from π^0 decay, wide-angle η decays, etc.) show that about 42% of the γ-trigger events are not in fact prompt photons. Accordingly, an appropriate amount of the π^0-trigger distribution (Fig. 9a) is subtracted from the γ-trigger sample (Fig. 9b) to produce the prompt-γ distribution shown in Fig. 9c, where no excess of tracks is seen above the uncorrelated-particle estimate. The same conclusion is reached from examining the rapidity difference between the trigger particle and same-side π^0's (Figs. 9d, e, f) and same side-π^0's having $p_T > 0.5$ GeV/c (Figs. 9g, h, i).

The CCOR collaboration looked at the fraction of events attributed to direct-photon production accompanied and unaccompanied by another particle [5]. Events with at least one charged or neutral particle (in addition to the trigger) with $p_T > 0.3$ GeV/c and within

the range $\Delta\phi = 90°$ and having pseudorapidity η in the range $-0.7 < \eta < 0.7$ were termed accompanied; other events unaccompanied. Figure 10 shows the fraction of such events as function of the transverse momentum of the trigger. The fraction of unaccompanied photons rises with p_T as expected. The fraction of accompanied photons is consistent with zero except for the highest data point at $p_T \approx 11$ GeV/c. Neglecting this last point for the moment, we see that the data are in qualitative agreement with photon production by the QCD diagrams. The last point, assuming it is a real effect, could be caused by the onset of significant quark bremsstrahlung (Fig. 2d), as has been recently suggested [15].

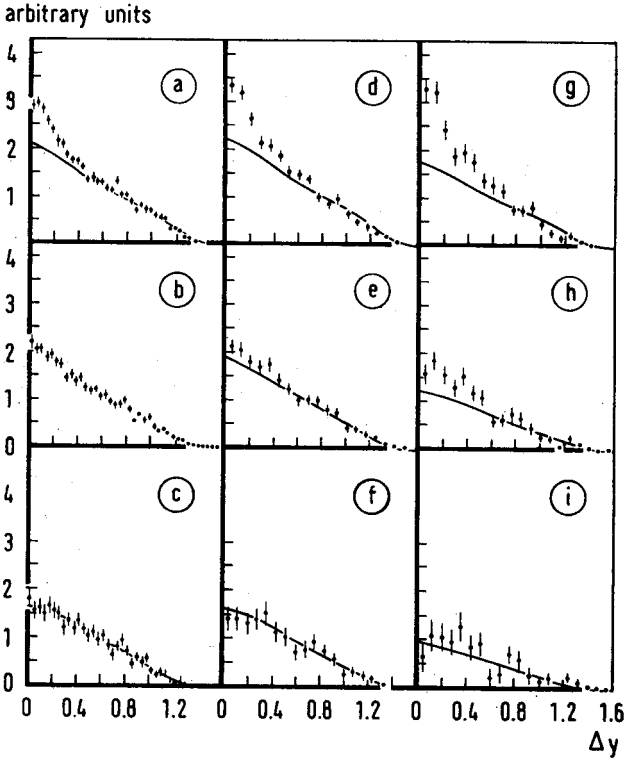

Fig. 9. The rapidity difference between charged tracks and the trigger (a) π^0, (b) γ-candidate, (c) pure γ; the rapidity difference between π^0's and the trigger (d) π^0; (e) γ-candidate, (f) pure γ; the rapidity difference between π^0's with $p_T > 0.5$ GeV/c and the trigger (g) π^0, (h) γ-candidate, (i) pure γ. The curves are the expected distributions assuming uncorrelated particles produced uniformly in rapidity [13]

In p–p collisions antiquarks must come from the sea. Consequently, the inverse Compton process (Fig. 2b) is dominant over the annihilation process (Fig. 2c) as we have seen in Fig. 8. Since the quark charge squared enters the cross section and since there are twice as many u as d valence quarks, we expect (neglecting the sea) ug → uγ to be eight times more frequent than dg → dγ. This should result in more positive than negative tracks on the away side. CCOR [5] finds R = (*number of positive particles*) / (*number of negative particles*) $\approx 4 \pm 1.4$ for direct photons but only $\approx 1.8 \pm 0.2$ for a π^0 trigger at $p_T \approx 10$GeV/c, in qualitative agreement with the expectation. However better statistics are clearly needed.

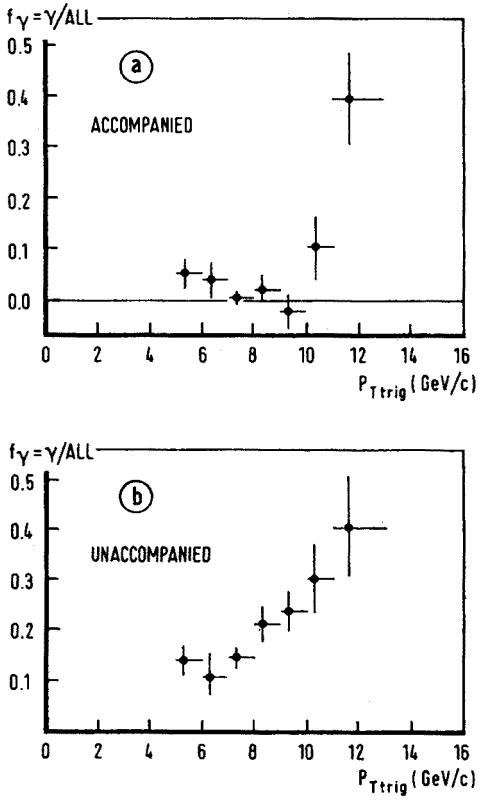

Fig. 10. The fraction of events attributed to direct photon production vs. $p_{T\,\text{trigger}}$ for those events where the trigger (a) was and (b) was not accompanied by another particle in the trigger hemisphere [5]

2.4. Conclusions

The data establish the existence of prompt photons, which are required by QCD. Further, the experimental cross sections are in fairly good agreement with QCD calculations. However this apparent agreement can not yet be regarded as more than qualitative support for QCD, since the validity of the calculations is open to several questions: (1) The calculations depend greatly on what is assumed for the gluon structure function, which is poorly known. In the Drell-Yan process the gluon structure function enters the order α_s corrections. A recent experiment on high-mass μ-pair production [16] extracted $g(x) = 2.55\ (1-x)^{4.1\pm0.2}$ using a model [17] which included the order α_s corrections and a primordial k_T distribution and forcing the normalization $\int_0^1 g(x)dx = 0.5$. While calculations using $g(x) \sim (1-x)^4$ agree reasonably well with the prompt photon data (Fig. 7), particularly if soft gluon effects are included, it must be pointed out that the value of $4.1'\pm0.2$ is subject to systematic errors which are probably larger than the quoted 0.2 statistical error and to model assumptions. Determination of $g(x)$ in other experiments

would be very helpful. (2) The effect of higher order diagrams needs to be included. (3) The effects of higher twists need to be investigated. Inclusion of higher order terms and/or higher twists could affect the $g(x)$ needed to fit the data.

2.5. Future experiments

Apart from increased statistics, experiments in the near future will produce data using different beam particles and will examine better the features of the away-side jet. In particular it needs to be established that there indeed is a jet on the away side.

The use of different beam particles is particularly useful since the relative role of the annihilation and Compton diagrams depends on the antiquark content of the beam. As we have seen, in p–p interactions the Compton diagram dominates. However, the annihilation process will be important in π-beam experiments (and relatively more important in π^-–p than in π^+–p), increasing relative to the Compton process with increasing p_T since valence quark distributions are harder than the gluon distribution. In p–$\bar{p}$ experiments the annihilation process is still more strongly favored. Thus use of different beams provides further tests of QCD. Experimentally there are also advantages in looking at ratios such as $R = \sigma(\pi^-p \to \gamma X)/\sigma(\pi^+p \to \gamma X)$ rather than at the cross sections separately, since then systematic errors in absolute normalization will cancel, or at differences $D = \sigma(\pi^-p \to \gamma X) - \sigma(\pi^+p \to \gamma X)$, where systematic errors in γ/π^0 and γ/η will tend to cancel.

Study of the away-side jet is particularly interesting when different beam particles are available. As we have seen, in p–p production of prompt photons the away-side jet is predominantly a quark (mostly u) jet. In $\bar{p}$–p interactions it will be predominantly a gluon jet. Such experiments have the potential of investigating the difference between quark and gluon jets [18].

It is also worth noting that the production of two high-p_T prompt photons is also interesting. It proceeds by $q\bar{q}$ annihilation as in Fig. 2c but results in two photons instead of a photon plus a gluon. The structure function dependence is the same as Drell-Yan, but the QCD cross section and higher order corrections are different being related to the $q\bar{q} \to \gamma g$ process. In lowest order the two photon process is the same as the $q\bar{q} \to \gamma g$ process except that the cross section is a factor of about 130 smaller since it contains α instead of α_s and has a color factor of 1/3 instead of 8/9 (coming from the sum over outgoing and averaging over incoming colors). This lower cross section will make the process more difficult to detect. But if it can be detected it has the advantage of simpler interpretation since there is only one lowest order diagram and since there is no jet fragmentation.

3. High p_T hadron production

3.1. Introduction

As discussed in Section 1, high p_T hadrons are thought to be produced via hard, binary parton interactions with the other partons in the interacting hadrons playing a spectator role. This picture, as shown pictorially in Fig. 11, gives rise to four jets, two at high

p_T and two spectator jets. Since the cross sections for these processes are small it is necessary to use a trigger so that only events containing high-p_T particles will be recorded. The first such trigger employed was a single-particle trigger. Conceptually (see Fig. 11) this is a small device placed at a reasonably large angle which measures the momentum of a particle passing through it. Only if this momentum is larger than some preset value is

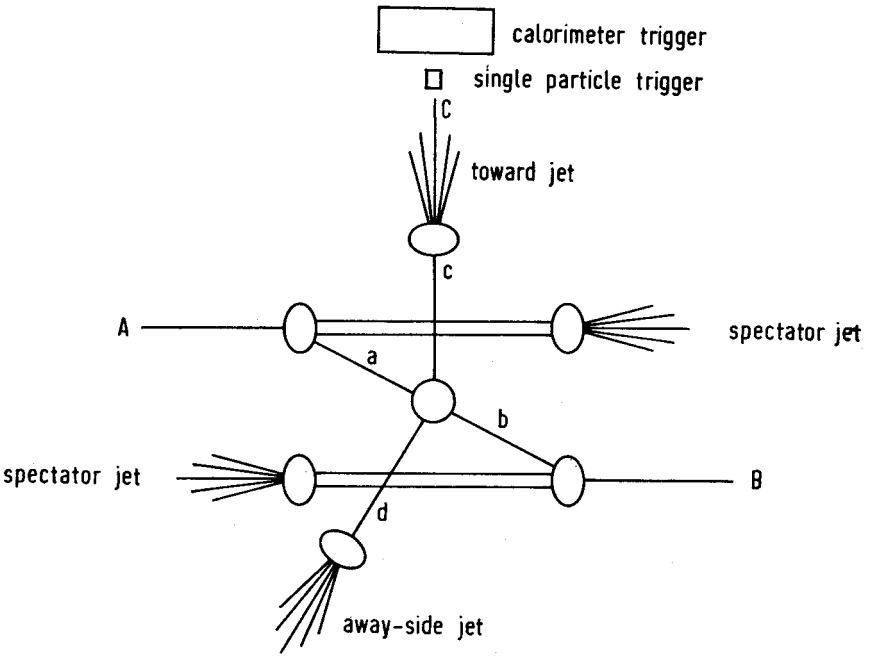

Fig. 11. Pictorial representation of high-p_T hadron production

the event recorded. The invariant cross section for the reaction thus measured A+B $\rightarrow$ C+X which is assumed to proceed through the subprocess a+b $\rightarrow$ c+d is given, neglecting initial parton transverse momentum, by [19]:

$$E_C \frac{d^3\sigma}{dp_C^3} = \frac{1}{\pi} \int_{x_{a,\min}}^{1} dx_a \int_{x_{b,\min}}^{1} dx_b P_A^a(x_a) P_B^b(x_b) \frac{d\sigma(ab \rightarrow cd)}{d\hat{t}} \frac{1}{z} D_c^c(z), \qquad (1)$$

where the longitudinal momentum fractions are $x_a = p_a/p_A$, $x_b = p_b/p_B$ and $z = p_C/p_c$. The Mandelstam variables of the subprocess are given by $\hat{s} = x_a x_b s$, $\hat{t} = x_a t/z$, and $\hat{u} = x_b u/z$. The lower limits of integration are determined by the condition $\hat{s}+\hat{t}+\hat{u} = 0$ and $z = -(u/x_a + t/x_b)/s \leqslant 1$ to be $x_{a,\min} = -u/(s+t)$ and $x_{b,\min} = -x_a t/(x_a+u)$. The parton distributions are denoted by P: $P_A^a(x_a)$ is the probability of finding a parton of type a with momentum fraction x_a in hadron A. The fragmentation function $D_c^C(z)$ gives the probability that a parton of type c will fragment to a hadron C having momentum fraction z. The functions P and D should be the same as found in other experiments such

as deep inelastic lepton scattering or (for D) e^+e^- annihilation and (for P) the Drell-Yan process.

In naive parton models where P and D are assumed to scale and the subprocess to be quark-quark scattering via vector exchange (photon or gluon) $d\sigma/d\hat{t} \sim s^{-2} \sim p_T^{-4}$. Consequently, scaling behavior

$$E\frac{d^3\sigma}{dp^3} \sim p_T^{-n} f(x_T, \cos\theta^*) \tag{2}$$

with $n = 4$ was expected [20]. The early data ($p_T \lesssim 6$ GeV/c) showed, however, a p_T^{-8} dependence. We shall return to this point later.

3.2. Evidence of jet structure

Let us now briefly list the evidence for the jet structure implied by the above picture [21]: The trigger particle shows a strong azimuthal correlation with away-side particles but little or no correlation in rapidity. On the other hand, away-side particles are correlated with the fastest away-side particle, and this correlation increases with the p_T of the fastest

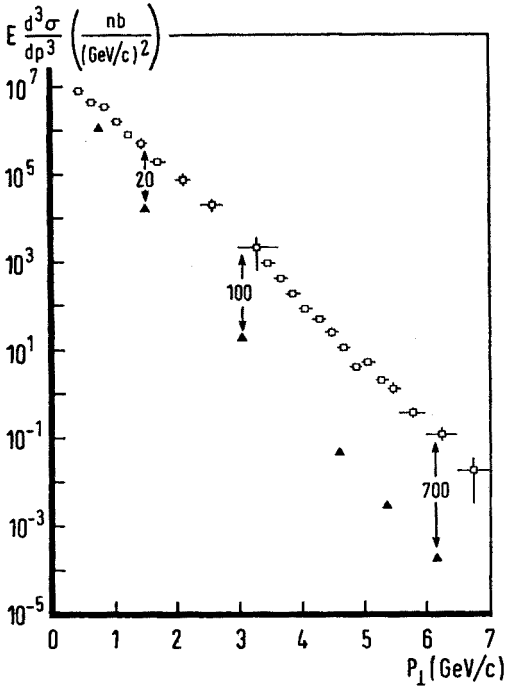

Fig. 12. Invariant cross section for pp → jet + X (squares) compared with single particle production (triangles) [22]

particle. This is suggestive of jets which fragment with limited transverse momentum. Although the toward jet is strongly biased by the trigger towards jets which fragment such that one particle receives most of the momentum of the parton, the away jet is not. Properties of the away jet have been compared with jets produced in e^+e^- and νp interactions.

The multiplicity dependence on energy is similar although it is systematically somewhat higher for the hadron-hadron case. The fragmentation functions agree very well. The transverse momentum (with respect to the jet axis) distribution is also in reasonable agreement. We can conclude that there is a jet on the away side with properties similar to jets in e^+e^- and νp interactions.

Having gained support for the jet picture, we can replace the single particle trigger by a calorimeter trigger (Fig. 11). A calorimeter is a device which measures the total energy of the particles entering it. By choosing a calorimeter of appropriate size so that all of the particles of the jet will enter it and thus triggering on the jet energy, the above-mentioned trigger bias can be removed (or at least greatly reduced). As would be expected the jet cross sections are much larger than single-particle cross sections as function of p_T as is seen in Fig. 12. The use of a jet trigger has the calculational simplicity that the fragmentation function does not have to be known; in Eq. (1) D_C^c is replaced by $\delta(1-z)$.

Another bias has not yet been mentioned, namely the preference for events where the initial partons had a net transverse momentum in the trigger direction or where an upward statistical fluctuation occured in the calorimeter response. This bias is not removed by using a jet trigger, but can be reduced by a two-jet (or double-arm) trigger where a second calorimeter is placed on the away side. The trigger is than on the sum of the energies found in the two calorimeters. However, such a set-up imposes an angular relationship between the two jet directions.

3.3. Perturbative QCD

In perturbative QCD collinear gluon diagrams are taken into account to all leading log orders in α_s by making the structure functions and fragmentation functions Q^2-dependent. However, in taking these functions over from deep inelastic lepton-nucleon experiments it is not clear what quantity to use for Q^2 [19]. Common choices for Q^2 are $-\hat{t}$, $(\hat{s}\hat{t}\hat{u})^{1/3}$, $2\hat{s}\hat{t}\hat{u}/(\hat{s}^2+\hat{t}^2+\hat{u}^2)$, or simply $4p_T^2$. Different choices of Q^2 combined with uncertainty in the gluon distribution cause lowest order cross section calculations to disagree by an order of magnitude at SPS/FNAL energies. An additional difficulty for the fragmentation functions arises from a different color structure of the fragmenting systems. In deep-inelastic lepton-nucleon scattering and in e^+e^- annihilation the fragmenting systems (quark-diquark and quark-antiquark, respectively) form a color singlet, while in high-p_T hadron production the two partons responsible for the high-p_T jets may or may not be in a color singlet. Their fragmentation could thus be influenced by the spectator quarks.

In addition to the $qq \to qq$ process of the naive parton model, several other processes may occur (Fig. 13). The cross-section formula (1) must then be summed over all subprocesses, each of which involves different structure functions, different fragmentation functions, and different $\hat{t}$- and $\hat{u}$-dependence, and hence a different p_T-dependence. An example of such a calculation [23] is shown in Fig. 14. The relative importance of $q\bar{q}$ processes will be greater in π–p reactions where the beam particle contains a valence antiquark. At the highest values of p_T the $qq \to qq$ subprocess dominates. We should there-

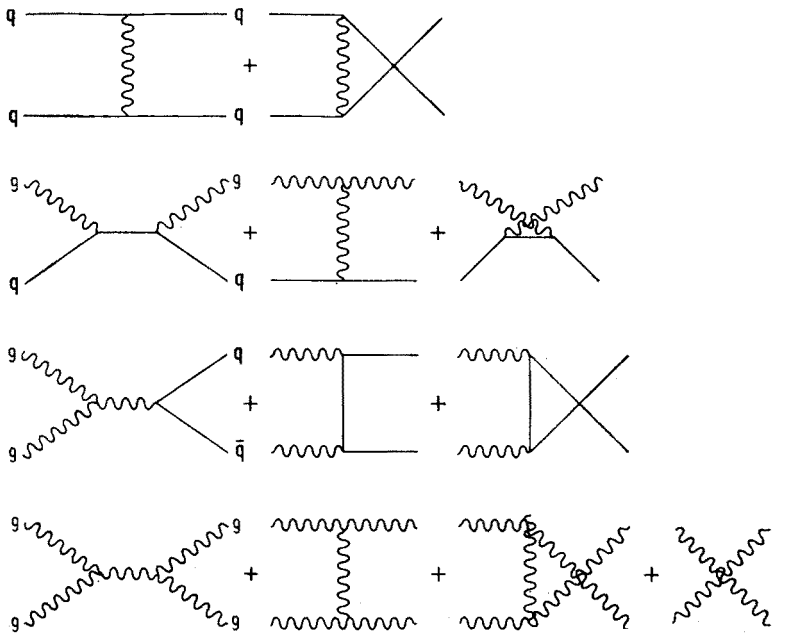

Fig. 13. Lowest-order subprocesses contributing to high-p_T hadron production. Similar subprocesses involving $\bar{q}$ instead of q are not shown

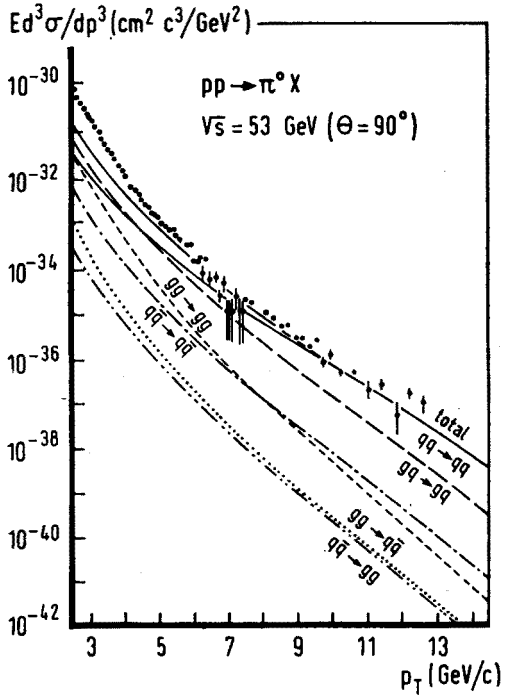

Fig. 14. QCD predictions compared with data for $pp \to \pi^0 X$ at $\theta^* = 90°$ and $\sqrt{s} = 53$ GeV [23]. The contributions of the various subprocesses are shown

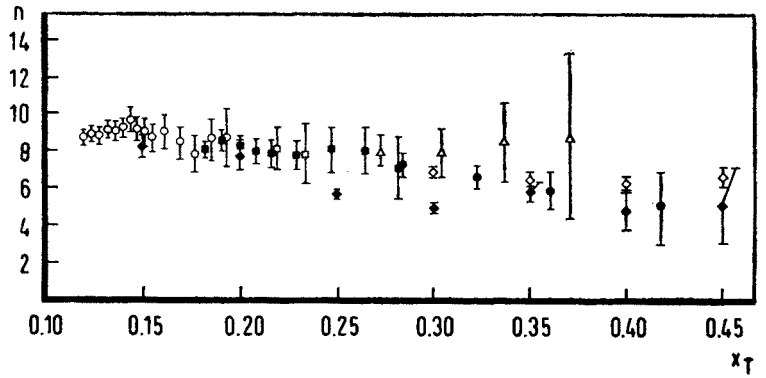

Fig. 15. The effective scaling parameter $n(x_T, s)$ of equation (2) as function of $x_T = 2p_T/\sqrt{s}$ as found in $pp \to \pi^0 X$ at the ISR by the AABC collaboration [24] (circles, crosses, squares and triangles) and by the CCOR collaboration [25] (open and closed diamonds). The AABC points have only statistical error bars; there is in addition a systematic error on n of ± 0.7

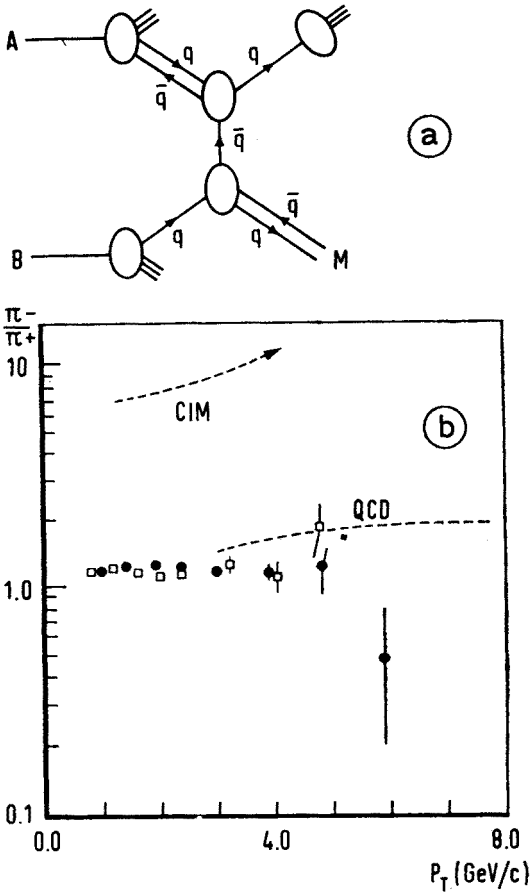

Fig. 16. (a) A diagram involving a typical CIM subprocess qM → qM, which contributes as p_T^{-8} to the single inclusive high-p_T cross section. (b) The π^-/π^+ ratio measured in $\pi^- p \to \pi X$ at $y = 0$ as function of p_T at 200 and 300 GeV/c [28] compared to the results of a CIM model [29] and a QCD model [30]

fore expect a p_T^{-4} scaling behavior to set in. As seen in Fig. 15 there is some suggestion of this.

Higher-order processes may also be important although at present the situation is not completely clear. $O(\alpha_s^3)$ corrections have been calculated only for quark-quark scattering of different-flavor quarks. The conclusion of Ref. [26] was that the corrections are very large. It has been pointed out [27] that these terms can be minimized by an appropriate choice of the renormalization and factorization prescriptions. However, in making comparisons with high-p_T data, the structure functions used must have been obtained from deep inelastic scattering or Drell-Yan data using QCD formulae calculated (to sufficiently high orders) using the same prescriptions. Nevertheless, the choice of scale variable, i.e. Q^2, is free and should be chosen so as to minimise the importance of higher-order terms.

The situation appears better with respect to higher twists. The constituent intercharge model (CIM) was originally invoked to explain the p_T^{-8} scaling behavior. Naively, one would expect CIM diagrams to contribute asymmetrically to charged meson production. For example, a π^- beam would be expected to produce more high-p_T π^- mesons than π^+ mesons through the subprocesses shown in Fig. 16a. The results [28] of a Chicago-Princeton measurement of the π^-/π^+ ratio from π^-p collisions are shown in Fig. 16b together with the predictions of a CIM model [29] and of a QCD model [30]. Strong CIM contributions can clearly be ruled out, even at quite low values of p_T.

3.4. Initial parton transverse momentum

If we assume that the initial partons can have non-zero transverse momentum, equation (1) is modified to include a transverse momentum distribution and an integral over the transverse momentum for each parton. Some transverse momentum arises simply through the uncertainty principle. The average value of the transverse momentum is then related to the size of the hadron and should be of the order of 300 MeV/c. Further, the transverse momentum is independent of the longitudinal momentum fraction x and should follow a normal distribution. In addition there may be a non-perturbative, "primordial" parton transverse momentum associated with confinement. It is not at all obvious that such contributions to the parton transverse momentum are either independent of x or normally distributed. Nevertheless, the approach taken so far in calculations is to assume a Gaussian form for the transverse momentum in the structure and fragmentation functions with the average value of the transverse momentum $\langle k_T \rangle$ being a free parameter to be determined from experiment.

Calculations [32] including these effects greatly improve agreement with experiment (Fig. 17), particularly at low values of p_T and help to explain the p_T^{-8} scaling behavior there. The value of $\langle k_T \rangle$ needed, roughly 800–1000 MeV/c, is much larger than expected from the uncertainty principle and the size of the nucleon, though roughly consistent with values found in Drell-Yan experiments using a similar parametrization [2]. In view of the above-mentioned uncertainties in the cross-section calculations one should not place too much importance on this result.

The transverse momentum of the initial partons can also be studied by looking at p_{out}, the component of momentum of particles in the away-side jet perpendicular to the beam-trigger plane. Assuming the picture that high-p_T particles are produced only via $2 \rightarrow 2$ parton scattering, p_{out} is non-zero because of two effects: the initial parton trans-

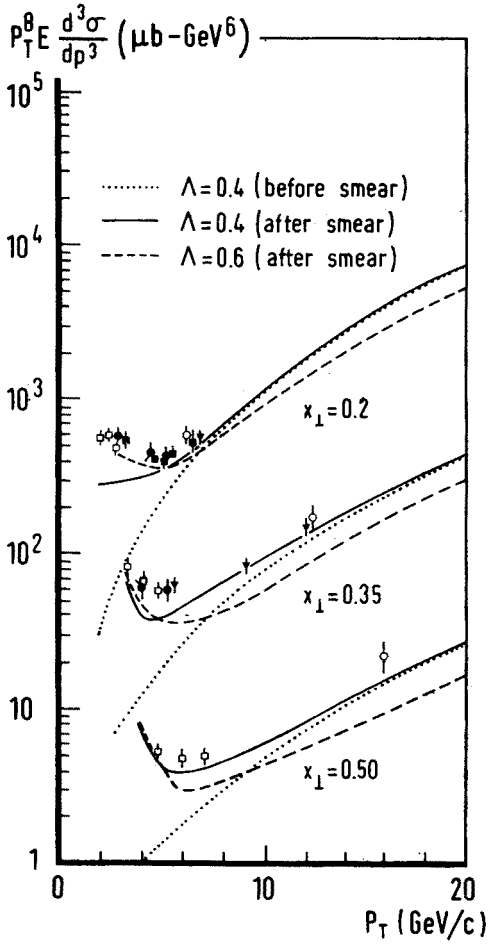

Fig. 17. $p_T^8 \cdot Ed^3\sigma/dp^3$ versus p_T at fixed $x_T = 2p_T/\sqrt{s}$ for $pp \rightarrow \pi X$ at $y = 0$ [31] compared to QCD calculations [32] showing the effect of including parton transverse momentum. The structure and fragmentation functions were parametrized as Gaussian distributions in k_T with $\langle k_T \rangle$ chosen as 848 and 439 MeV, respectively

verse momentum k_T and the transverse momentum acquired in the parton fragmentation j_T. The CCOR collaboration has analysed its $pp \rightarrow \pi^0 X$ high-p_T data in the following way [33]: The quantity

$$x_E = -\boldsymbol{p}_{T\,\mathrm{track}} \cdot \boldsymbol{p}_{T\,\mathrm{trigger}} / |\boldsymbol{p}_{T\,\mathrm{trigger}}|^2$$

approximates $z = p_{||}/p_{jet}$ becoming equal to z for $p_{jet} = -p_{T\,trigger}$. Making use of this it has been shown [34] that

$$\langle |p_{out}| \rangle^2 \approx 2\langle |k_{Ty}| \rangle^2 x_E^2 + \langle |j_{Ty}| \rangle^2 (1 + x_E^2), \tag{3}$$

where $\langle |k_{Ty}| \rangle$ and $\langle |j_{Ty}| \rangle$ are the average values of the components of k_T and j_T out of the scattering plane. For small x_E, p_{out} is kinematically limited to small values. The analysis is therefore done using only tracks with $p_T > 1.4$ GeV/c. For different regions of x_E, $\langle |p_{out}| \rangle$

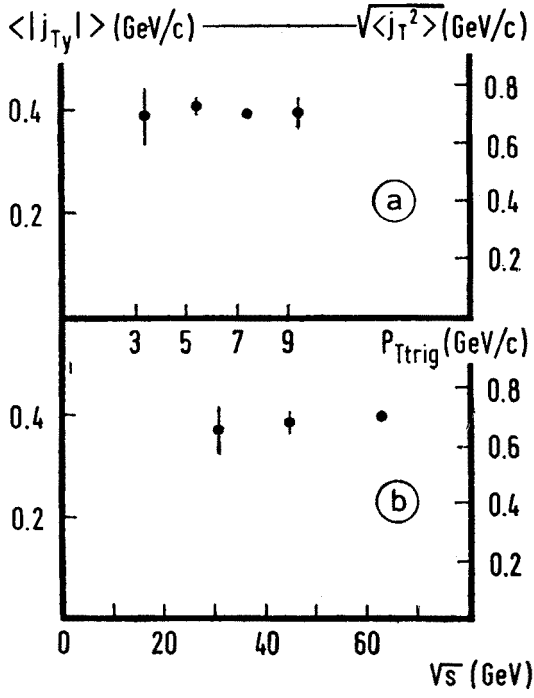

Fig. 18. The average fragmentation transverse momentum as function (a) of $p_{T\,trigger}$ and (b) of s as found in $pp \to \pi^0 X$ by the CCOR collaboration [33]

is evaluated, and a fit is done to Eq. (3). The results show (Fig. 18) that $\langle |j_{Ty}| \rangle$ is independent of $p_{T\,trigger}$ and of s, consistent with the model assumptions. Assuming then a Gaussian shape for j_{Ty} and that j_{Tx} has the same distribution, they find $\langle j_T^2 \rangle^{1/2} = 0.70 \pm 0.01$ GeV/c, which is somewhat higher than the value 0.55 GeV/c found in e^+e^- experiments using only the high-momentum hadrons [35]. On the other hand, $\langle k_{Ty} \rangle$ is found to increase with both $p_{T\,trigger}$ and s. The systematic uncertainties are different if one uses only events where $x_E \sim 1$, i.e. where the total transverse momentum of the away-side charged particles balances the trigger transverse momentum. Then equation (3) leads to

$$\langle \Sigma |p_{out}| \rangle^2 = 2\langle |k_{Ty}| \rangle^2 + \langle |j_{Ty}| \rangle^2. \tag{4}$$

Using the value of $\langle|j_{Ty}|\rangle$ found using Eq. (3), $\langle|k_{Ty}|\rangle$ is then found using Eq. (4). These values (see Fig. 19) agree reasonably well with those found from Eq. (3) directly. They correspond, assuming the same Gaussian distribution for k_{Tx} as for k_{Ty}, to $\langle k_T\rangle$ varying from ~ 0.6 to ~ 1.3 GeV/c, the same order of magnitude suggested by the cross-section calculations. The rise of $\langle k_T\rangle$ with p_T and s is suggestive of a constant primordial k_T plus a contribution from gluon emission which was not taken into account in the analysis.

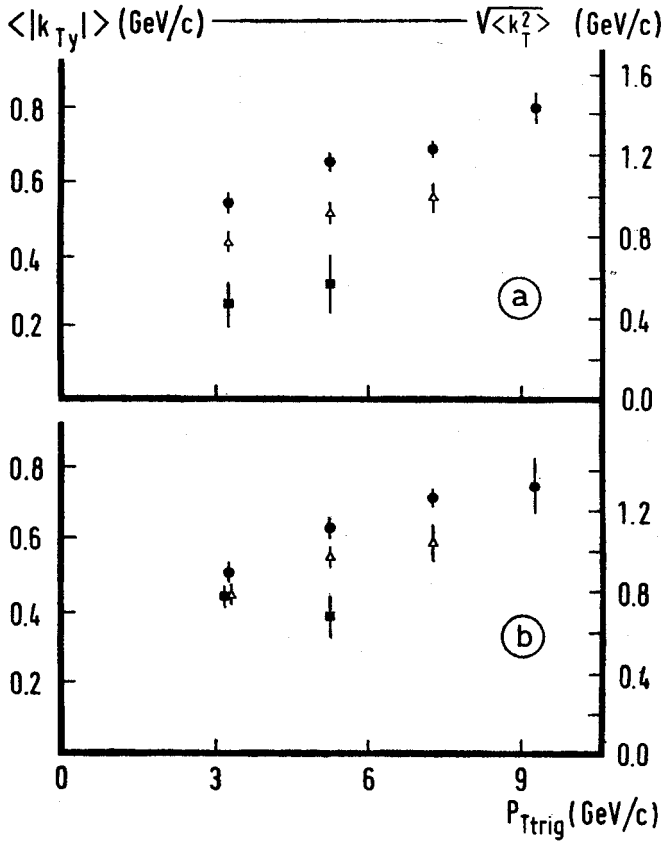

Fig. 19. The average transverse momentum of the incident partons as function of the p_T of the trigger particle as found [33] using Eq. (4) in pp → π^0X at $\sqrt{s} = 31$ (squares), 45 (triangles), and 62 (circles) GeV [33]

Initial parton k_T has also been examined at FNAL using a double-arm calorimeter trigger [36]. With a calorimeter on each side, the experiment triggered on $|p_{T\,\mathrm{left}}| + |p_{T\,\mathrm{right}}|$. The difference between the left and right calorimeter signals is then a measure of k_{Ty}. As may be seen in Fig. 20, $\langle k_T\rangle$ is around 1 GeV/c [36]. This experiment also found an increase of $\langle k_T\rangle$ with p_T.

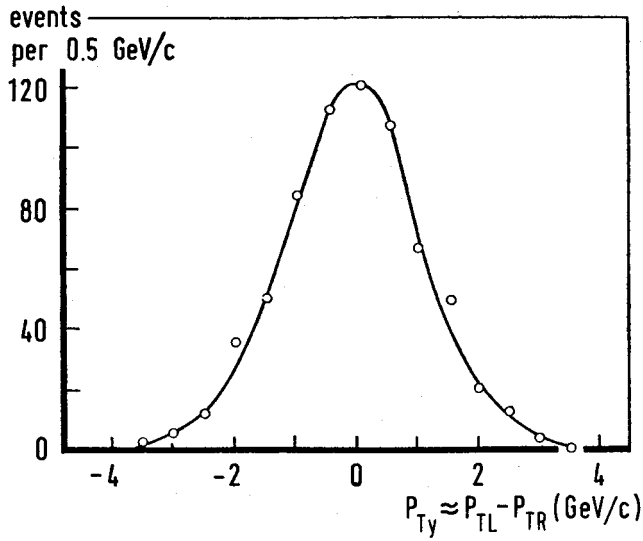

Fig. 20. Difference in p_T between the left and the right calorimeters for events where $|p_{T\,left}| + |p_{T\,right}| = 6.0$ to 6.5 GeV/c in pp collisions at 200 GeV/c [36]

3.5. Large acceptance calorimeter experiments

The results examined thus far have come from experiments with single-particle, one-arm or two-arm triggers. The single-particle trigger suffers from biases in favor of trigger jets where one particle receives most of the fragmenting parton's momentum and for events where k_T is towards the trigger. The one-arm trigger is biased in favor of narrow trigger jets and has the same k_T bias as the single-particle trigger. The two-arm trigger

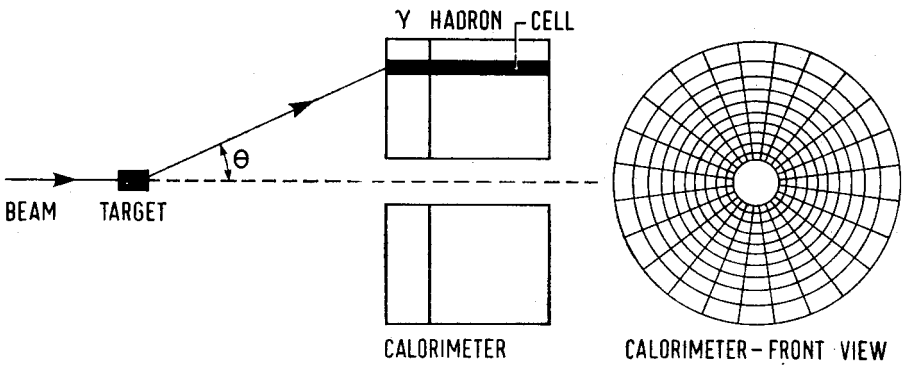

Fig. 21. The transverse energy trigger of the NA5 experiment

is biased towards events where both jets are narrow and also have a fixed angular separation.

To overcome the narrow-jet bias as well as the k_T bias, a calorimeter trigger having large acceptance in rapidity and full azimuthal acceptance has been proposed. Triggering

on the total transverse energy $E_T = \Sigma|p_T|$, such a trigger is not biased towards the four-jet picture. Observance of jets in such events would establish the correctness of this picture. The first to use such a trigger was the NA5 (Bari-Cracow-Liverpool-MPI Munich-Nijmegen Collaboration) experiment at CERN [37]. More recently two ISR groups, R416 (CERN-Collège de France-Dortmund-Heidelberg-Warsaw Collaboration) using the split-field magnet (SFM) [38] and R807 (Brookhaven-CERN-Niels Bohr-Lund-Rutherford-Tel Aviv Collaboration) using the axial-field spectrometer (AFS), [39] have analyzed their minimum-bias trigger events simulating the NA5 trigger in software.

The NA5 trigger (Fig. 21) is provided by a cylindrical calorimeter of 3 meter diameter whose axis coincides with the beam. A hole in the calorimeter allows low-p_T forward particles to pass through. The calorimeter is divided into an electromagnetic and a hadron section. It consists of 10 radial rings each of which is divided into 24 azimuthal-cells, the size of the cells varying with the radius such that each cell subtends approximately the same CMS solid angle ($\Delta\theta^* \approx 9°$, $\Delta\phi \approx 15°$). Each of the 480 cells is individually read out using wave-length shifting acrylic rods [40] providing a signal E^i. The total transverse energy which is used as the trigger is then a sum over calorimeter cells:

$$E_T = \Sigma \sin\theta_i(E_i^{em} + E_i^{hadron})$$

which for relativistic particles is approximately $\Sigma|p_T|$. The calorimeter was positioned such that the polar angular acceptance was $45° < \theta^* < 135°$ corresponding, after imposition of a fiducial region, to $-0.88 < y < 0.67$ for a 300 GeV/c beam. Three trigger configurations were used: (1) full calorimeter where the sum extends over all cells, (2) double-arm where the sum extends only over cells with $0° < \phi < 90°$ or $180° < \phi < 270°$, and (3) single-arm where the sum extends only over one quadrant of the calorimeter $0° < \phi < 90°$.

The AFS and SFM both have (nearly) 2π azimuthal acceptance and good momentum analysis for charged particles produced centrally. They analysed events taken with a minimum bias trigger (an interaction trigger with about 95% efficiency) in terms of $E_T = \Sigma(p_T^2 + m^2)^{1/2}$ of charged particles produced centrally with $|y| < 0.8$ (AFS) and $|y| < 0.75$ (SFM).

3.5.1. Preliminary results

The results [37,41] of all three experiments are preliminary. The NA5 data are compared to two models:

(1) A four-jet model having two large-p_T jets and two forward-backward spectator jets. The cross sections are calculated using QCD matrix elements for two-constituent scattering, structure functions taken from νN and Drell-Yan experiments, including scale breaking, and $\alpha_s = 12\pi/25 \log(1 + Q^2/\Lambda)^2$ with $\Lambda = 0.2$ GeV and $Q^2 = 4p_T^2$. Primordial parton k_T was included with $\langle k_T^2\rangle^{1/2} = 1.2$ GeV/c. The partons were fragmented following the Field-Feynman prescription such that each of the two jet systems resembles jets in e^+e^- collisions. In this model with the full calorimeter trigger $E_T > 12$ GeV about 93% of the p_T of the two high-p_T jets is seen by the calorimeter and about 40% of the E_T in the calorimeter comes from particles in the spectator jets.

(2) A low-p_T cluster model which includes leading particles. Clusters are generated uniformly in rapidity with an exponential p_T distribution and an average mass of about

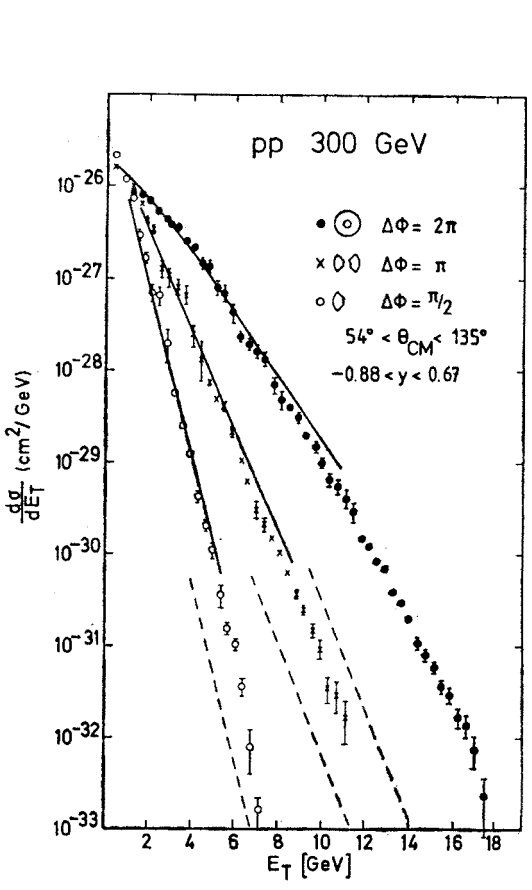

Fig. 22

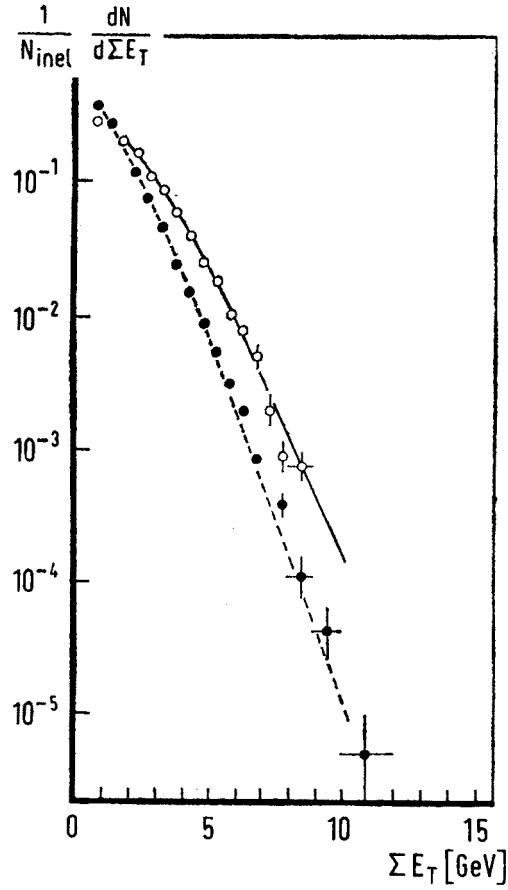

Fig. 23

Fig. 22. Cross sections versus trigger transverse energy for the full calorimeter trigger (full circles), the double-arm trigger (crosses), and the single-arm trigger (open circles) as found in the NA5 experiment for p–p interactions at 300 GeV/c. The low-p_T cluster and QCD-4-jet model predictions are shown with full and dashed lines, respectively

Fig. 23. Event rates versus total transverse energy of charged particles having $|y| < 0.8$ in a 92% azimuthal acceptance for pp interactions at $\sqrt{s} = 63$ GeV (full circles) and $\alpha\alpha$ interactions at $\sqrt{s} = 126$ GeV (open circles) in the R807 experiment. They are compared to a phase space model

2 GeV. They decay isotropically with an average charge multiplicity of about 2.5. An overall KNO multiplicity distribution was enforced. The final particles have $\langle p_T^2 \rangle^{1/2} = 0.36$ GeV/c. The cross sections are normalized to the total inelastic cross section. This model reproduced well the features of low-p_T events observed in bubble chamber experiments. The calorimeter resolution and acceptance were included in both models.

The cross sections $d\sigma/dE_T$ are shown for the NA5 data in Fig. 22. At large values of E_T the full calorimeter trigger cross section is roughly 100 times that of the double-arm

trigger. If four-jet events were dominant this factor would be much smaller since the acceptance differs only by a factor 2. The full calorimeter trigger cross sections are 10–100 times larger than that predicted by the four-jet model, the difference increasing with E_T. The double-arm trigger cross sections are also significantly above the four-jet model predictions. On the other hand, the low-p_T cluster model seems to agree with the data

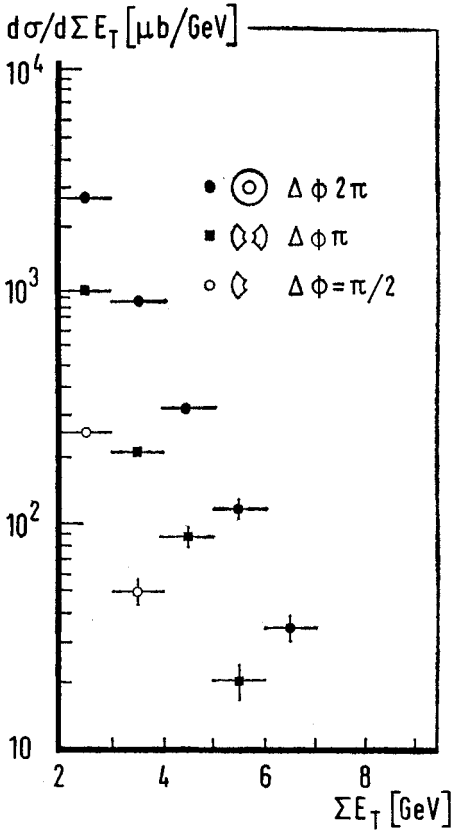

Fig. 24. Cross sections versus total transverse energy of charged particles having $|y| < 0.75$ and within azimuthal acceptance regions of 2π (full circles), π (squares), and $\pi/2$ (open circles) for pp collisions at $\sqrt{s} = 63$ GeV in the R416 experiment

for all three triggers. The cross sections for the ISR experiments are shown in Figs 23 and 24. The AFS results (Fig. 23) on p–p and α–α scattering agree with a phase space model containing independent particle emission and a KNO multiplicity distribution.

The scaling behavior of the π^-p cross section was investigated by the NA5 collaboration using the parametrizations

$$E\frac{d^3\sigma}{dp^3} \sim p_T^{-n} f(x_T) \quad \text{with} \quad x_T = \frac{2p_T}{\sqrt{s}} \tag{5}$$

and

$$\frac{d\sigma}{dE_T} \sim E_T^{-n} f(x_T) \quad \text{with} \quad x_T = \frac{E_T}{\sqrt{s}} \tag{6}$$

for the single-arm and full calorimeter triggers, respectively. For the single-arm trigger n seems to rise with x_T, as is shown in Fig. 25, consistent with FNAL experiment E260 results [42] and contrary to the expectations of QCD models which expect n to decrease

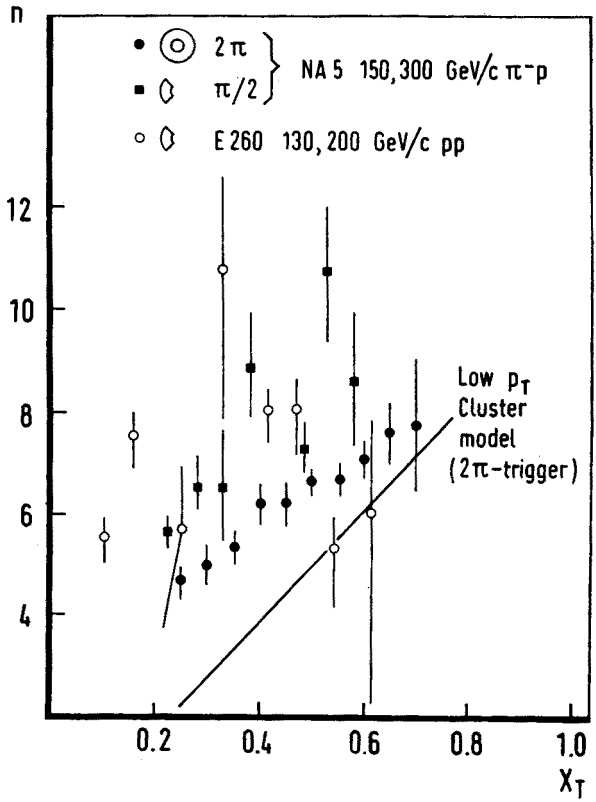

Fig. 25. The scaling parameter n of cross sections measured by the NA5 experiment with the full and single-arm calorimeter triggers. Results from the FNAL experiment E260 [42] are shown for comparison. Also shown is the prediction for the full calorimeter trigger of the low-p_T cluster model described in the text

with x_T, approaching $n = 4$ as indeed was seen in single-particle trigger experiments (Fig. 15). The full-calorimeter trigger data also rise roughly linearly with x_T. This is the sort behavior predicted by the low-p_T cluster model, although the values of n in this model lie below the data.

We now turn to the structure of the high-p_T events. The NA5 collaboration performed a planarity analysis in the transverse plane using the transverse momenta derived from energy clusters in the calorimeter. The planarity was defined as $P = (a-b)/(a+b)$ where a and b are the sum of the squares of the transverse momenta projected onto axes which

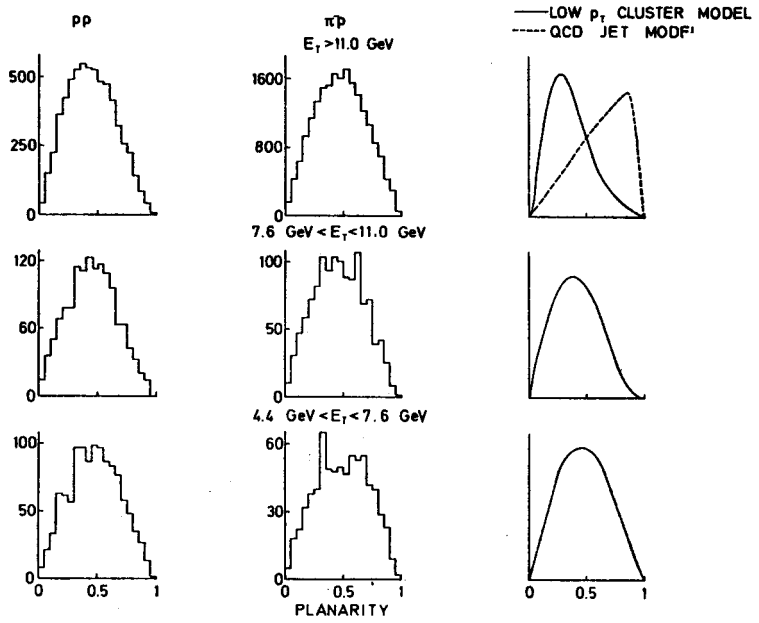

Fig. 26. Planarity distributions of events selected by the NA5 full-calorimeter trigger for π^-p and pp interactions at 300 GeV/c for different trigger thresholds. For comparison, the planarity distributions expected from the low-p_T cluster model and the QCD 4-jet model are also shown

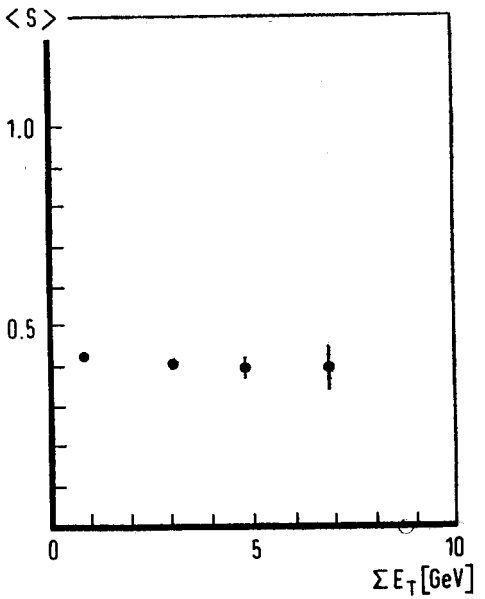

Fig. 27. The mean circularity $\langle S \rangle$ for charged particle multiplicities $n_{ch} > 4$ versus the trigger threshold ΣE_T as found in the R807 experiment

are chosen so as to maximize a and minimize b. Thus $P = 1 - S$ with S the two-dimensional analog of the sphericity, which we shall call the circularity. For an isotropic event $P = 0$ and for an event with pencil-like jets $P = 1$. Figure 26 shows the planarity distributions for 300 GeV/c π^-p and pp events with the full-calorimeter trigger for three different trigger thresholds. For comparison, the planarity distributions obtained from the low-p_T cluster model and the QCD jet model are also shown. The data appear to be somewhat less isotropic than predicted by the low-p_T cluster model for all thresholds. However, the data are much more isotropic than predicted by the QCD model. Also, the planarity

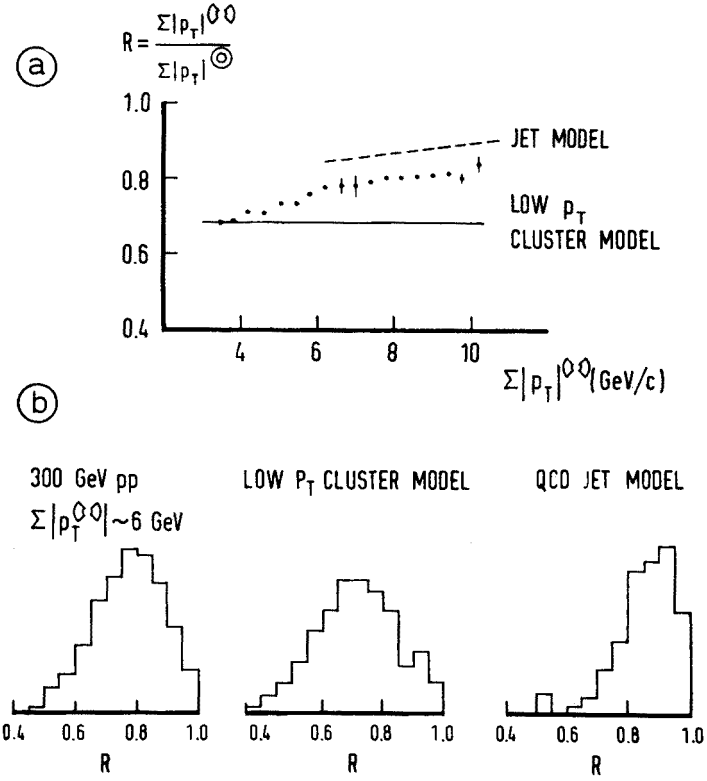

Fig. 28. The ratio of the transverse energy in the trigger arms to that in the entire calorimeter for a two-arm trigger in the NA5 experiment for pp interactions at 300 GeV: (a) the average value of this ratio as function of the transverse energy in the trigger arms and (b) the distribution of this ratio for a trigger of about 6GeV compared with the predictions of the low-p_T cluster model and the QCD four-jet model

distribution does not change very much with increasing transverse energy. This is also seen in the R807 experiment: As shown in Fig. 27, the mean circularity is too high for dominant jet structure and is independent of the transverse energy.

The two-arm trigger should preferentially select planar events. The NA5 collaboration examined the ratio of transverse energy in the trigger arms to that in the entire calorimeter. The ratio is found (Fig. 28) to lie between the predictions of the low-p_T and QCD models.

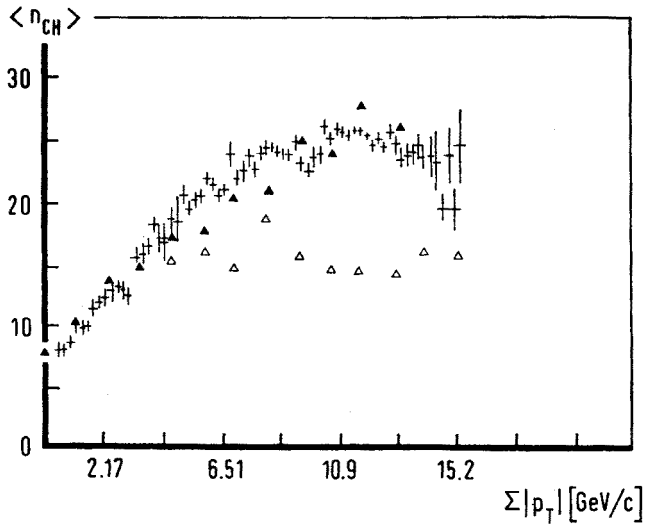

Fig. 29. The mean charged multiplicity as function of the trigger threshold as found for 300 GeV π^-p interactions using a full calorimeter trigger in the NA5 experiment compared with the predictions of the low-p_T cluster model (full triangles) and the QCD 4-jet model (open triangles)

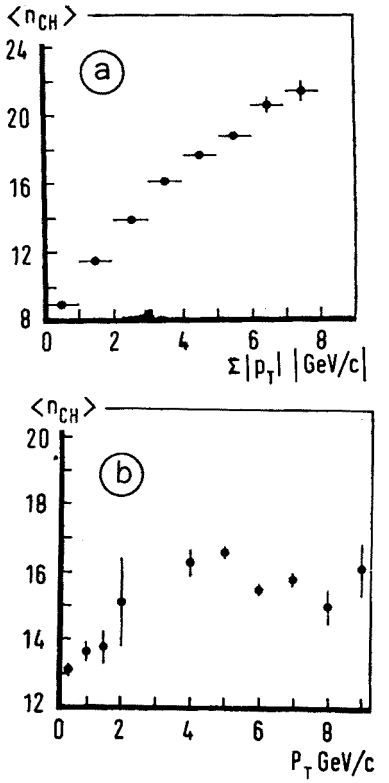

Fig. 30. The mean charged multiplicity measured in pp interactions at $\sqrt{s} = 63$ GeV in the R416 experiment (a) as function of the total transverse energy of charged particles and (b) as a function of the transverse momentum of a single particle emitted at $\theta \sim 52°$

Thus events selected with the two-arm trigger are also less jet-like than expected in the four-jet picture.

The charged particle multiplicity was determined in the NA5 experiment from runs where a streamer chamber surrounded the target. Figure 29 shows the mean multiplicity as function of the transverse energy seen by the full calorimeter. The multiplicity rises rapidly with transverse energy reaching a value of about 24 at around 8 GeV and then remains roughly constant. This behavior agrees with that predicted by the low-p_T cluster

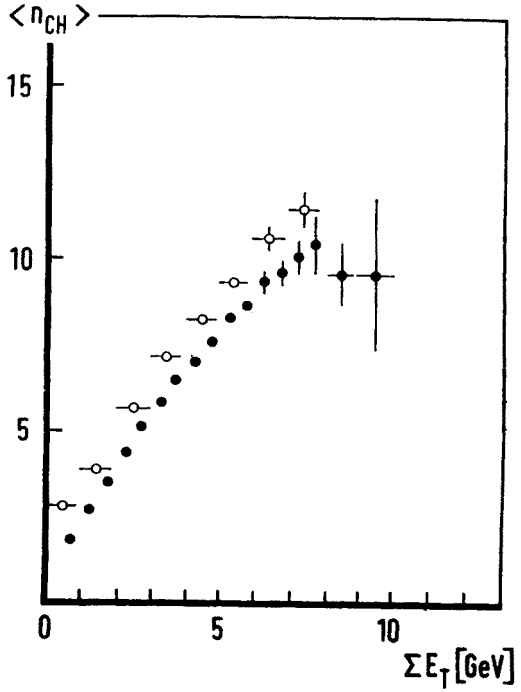

Fig. 31. The mean charged multiplicity within the acceptance versus the trigger threshold for pp interactions at $\sqrt{s} = 63$ GeV as found by the R416 experiment with $|y| < 0.75$ and full azimuthal acceptance (open circles) and the R807 experiment with $|y| < 0.8$ and 92% azimuthal acceptance (full circles)

model. The QCD four-jet model predicts much lower multiplicities. A similar rapid rise in multiplicity is observed by the R416 experiment when simulating the full-calorimeter trigger (Fig. 30a). However use of a single-particle trigger results in a multiplicity distribution (Fig. 30b) more as expected from a four-jet picture.

The charged particle multiplicity within the calorimeter acceptance was found by NA5 to be $\langle n_{ch} \rangle = 13 \pm 1$ for 300 GeV/c pp collisions with $E_T > 10$ GeV, which is between the prediction of the two models (15 for the cluster and 10 for the jet model, respectively). The ISR groups have looked at the rise of charged multiplicity within the acceptance as function of the total transverse energy of these particles (Fig. 31) and at the average total transverse energy as function of the number of charged particles within the acceptance (Fig. 32). The average multiplicity is seen to increase rapidly with ΣE_T, and

the average $\langle \Sigma E_T \rangle$ is seen to increase linearly with multiplicity. However $\langle n_{ch} \rangle = 10$ occurs for $\Sigma E_T \sim 7$ GeV, whereas $\langle \Sigma E_T \rangle = 7$ GeV corresponds to $n_{ch} \sim 14$. Thus the $\langle E_T \rangle$ per charged particle in the acceptance region is larger when triggering on ΣE_T than when triggering on n_{ch}.

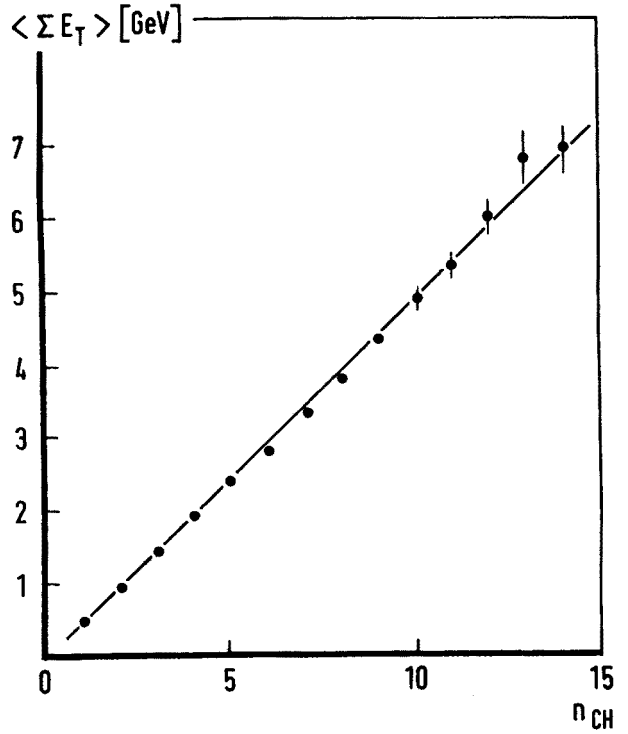

Fig. 32. The mean transverse energy of the charged particles as function of the number of charged particles as found by the R807 experiment for pp interactions at $\sqrt{s} = 63$ GeV

3.6. Conclusions

The data of the single-particle trigger experiments and of the FNAL one- and two-arm calorimeter trigger experiments are in qualitative agreement with the QCD four-jet picture. There is also reasonable quantitative agreement, but this may be fortuitous in view of uncertainties in the calculations. The many subprocesses involved make calculation of even the lowest order diagrams uncertain because of the lack of experimental input for such quantities as the gluon structure and fragmentation functions. Although these problems seem to disappear at the highest p_T where the $qq \to qq$ subprocesses should be dominant, the problem of higher order corrections remains. Nevertheless the jet picture provides, at present, the simplest qualitative interpretation of the data, in particular of the correlations.

The hope that unambiguous evidence for jets would be found using a large-transverse energy trigger has not been fulfilled. No evidence for a jet structure is found using such

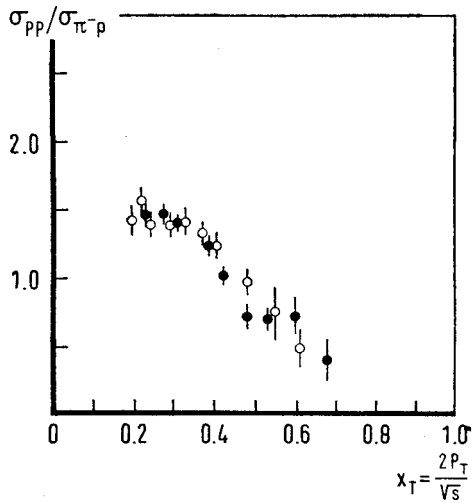

Fig. 33. The ratio of the pp and π^-p cross sections as functions of x_T obtained with a one-arm trigger in the FNAL experiments E260 (full circles) [44] and E395 [43] (open circles) at 200 GeV

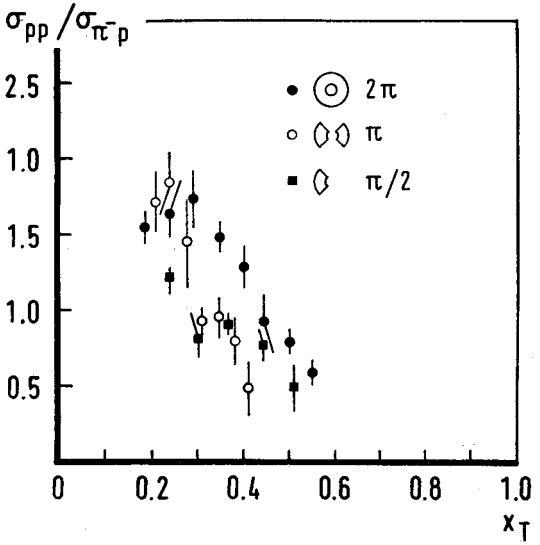

Fig. 34. The ratio of the pp and π^-p cross sections as function of x_T as found at 300 GeV in the NA5 experiment

a trigger; the events resemble in many ways the events of low-p_T (interaction trigger) experiments. The NA5 two-arm trigger results also do not appear jet-like. Nor do the cross sections of either the full or the two-arm trigger agree with a QCD four-jet model.

These results suggest that the interpretation of single-particle and one- and two-arm triggers should proceed with caution. As an example, we show in Fig. 33 the ratio of the pp and πp cross sections at 200 GeV as function of x_T obtained with a one-arm trigger in

the FNAL experiments E260 [44] and E395 [43]. The decrease in this ratio with x_T was interpreted as due to the harder π structure function which occurs because the π contains two valence quarks compared to the proton's three. This behavior was used [45] to extract the pion structure function using two-arm trigger data. But the NA5 data (Fig. 34) shows a very similar behavior for the full-calorimeter trigger data where there is no evidence for the jet picture.

I would like to express my thanks to the Organizing Committee of the VI School, and in particular to dr M. Zrałek, for inviting me to give these lectures and for a most enjoyable stay in Szczyrk.

REFERENCES

[1] S. D. Drell, T. M. Yan, *Phys. Rev. Lett.* **25**, 316 (1970); *Ann Phys.* **66**, 578 (1971).
[2] R. Stroynowski, *Phys. Rep.* **71**, 1 (1981); G. Matthiae, *Rivista del Nuovo Cimento* **4**, series 3, no. 1 (1981).
[3] P. Darriulat et al., *Nucl. Phys.* **B110**, 365 (1976); J. Cronin, *Hadron Induced Leptons and Photons*, Proceedings of the 1977 Lepton-Photon Conference, p. 579.
[4] M. Diakonou et al., *Phys. Lett.* **91B**, 296 (1980).
[5] A. L. S. Angelis et al., *Phys. Lett.* **98B**, 115 (1981).
[6] R. M. Baltrusaitis et al., *Phys. Lett.* **88B**, 372 (1979).
[7] F. Halzen, D. M. Scott, *Phys. Rev. Lett.* **40**, 1117 (1978).
[8] R. Ruckl, S. J. Brodsky, J. F. Gunion, *Phys. Rev.* **D18**, 2469 (1978).
[9] F. Halzen, D. M. Scott, *Phys. Rev.* **D18**, 3378 (1978).
[10] A. P. Contogouris, S. Papadopoulos, M. Hongoh, *Phys. Rev.* **D19**, 2607 (1979).
[11] A. P. Contogouris, S. Papadopoulos, J. Ralston, *Phys. Lett.* **B104**, 70 (1981).
[12] C. Kourkoumelis, Moriond Workshop on Lepton Pair Production, January 1981.
[13] F. Halzen, M. Dechantsreiter, D. M. Scott, Univ. of Wisconsin preprint COO-881-140.
[14] C. Kourkoumelis et al., *Nucl. Phys.* **B179**, 1 (1981).
[15] M. Dechantsreiter, F. Halzen, D. M. Scott, *Phys. Rev.* **D24**, 2856 (1981).
[16] A. S. Ito et al., *Phys. Rev.* **D23**, 604 (1981).
[17] G. Altarelli, G. Parisi, R. Petronzio, *Phys. Lett.* **76B**, 351 (1978); *Phys. Lett.* **76B**, 356 (1978); K. Kajantie, R. Raito, *Nucl. Phys.* **B139**, 72 (1978).
[18] M. Fontannaz et al., Ecole Polytechnique preprint A381.0380, March 1980; A. P. Contogouris, S. Papadopoulos, C. Papavassiliou, *Nucl. Phys.* **B179**, 461 (1981).
[19] See e.g. E. Reya, *Phys. Rep.* **69**, 195 (1981).
[20] S. M. Berman, J. D. Bjorken, J. Kogut, *Phys. Rev.* **D4**, 3388 (1971).
[21] This material has been covered in several reviews, e.g., P. Darriulat, *Ann. Rev. Nucl. Part. Sci.* **30**, 159 (1980).
[22] C. Bromberg et al., *Phys. Rev. Lett.* **43**, 565 (1979).
[23] J. F. Owens, E. Reya, M. Glück, *Phys. Rev.* **D18**, 1501 (1978).
[24] C. Kourkoumelis et al., *Z. Physik* **C5**, 95 (1980).
[25] A. L. S. Angelis et al., *Phys. Lett.* **79B**, 505 (1978).
[26] R. K. Ellis et al., *Nucl. Phys.* **B173**, 397 (1980); M. A. Furman, *Phys. Lett.* **98B**, 99 (1981).
[27] W. Furmański, W. Słomiński, Jagellonian University preprint, May 1980; William Celmaster and Dennis Sivers, Argonne National Lab. preprint ANL-HEP-PR-80-61, August 1980; W. Furmański, Jagellonian University preprint TPJU-11/81, May 1981.
[28] H. J. Frisch et al., *Phys. Rev. Lett.* **44**, 511 (1980).
[29] D. Jones, J. Gunion, *Phys. Rev.* **D19**, 867 (1979).
[30] R. D. Field, private communication cited in Ref. [28].

[31] B. Alper et al., *Nucl. Phys.* **B100**, 237 (1975); F. W. Büsser et al., *Nucl. Phys.* **B106**, 1 (1976); J. W. Cronin et al., *Phys. Rev.* **D11**, 2105 (1979); D. Antreasyan et al., *Phys. Rev. Lett.* **38**, 112, 115 (1977); A. G. Clark et al., *Phys. Lett.* **74B**, 267 (1978).
[32] R. D. Field, *Phys. Rev. Lett.* **40**, 997 (1978).
[33] A. L. S. Angelis et al., *Phys. Lett.* **97B**, 163 (1980).
[34] E. M. Levin et al., *Sov. Phys. JETP* **69**, 1537 (1975). R. P. Feynman, R. D. Field, G. C. Fox, *Nucl. Phys.* **B128**, 1 (1977).
[35] P. Söding, Proc. EPS International Conference on High-Energy Physics, Geneva, 1979, CERN, Geneva 1980, vol. 1, p. 271.
[36] M. D. Corcoran et al., *Phys. Rev. Lett.* **44**, 514 (1980); M. D. Corcoran et al., *Phys. Rev.* **D21**, 641 (1980).
[37] C. De Marzo et al., *Phys. Lett.* **112 B**, 173 (1982); C. Favuzzi et al., *High Energy Physics — 1980 (XX International Conference, Madison, Wisconsin)*, edited by L. Durand and L. G. Pondrom, American Inst. of Physics, New York 1981, part 1, p. 92; C. Favuzzi et al., submitted to XII International Symposium on Multiparticle Dynamics, Notre Dame, Ind., June 1981.
[38] W. Bell et al., *Nucl. Instrum. Methods* **156**, 11 (1978); B. Bouclier et al., *Nucl. Instrum. Methods* **115**, 235 (1974); B. Bouclier et al., *Nucl. Instrum. Methods* **125**, 19 (1975).
[39] H. Gordon et al., CERN-EP/81-34.
[40] V. Eckardt et al., *Nucl. Instrum. Methods* **155**, 389 (1978).
[41] K. P. Pretzl, Talk presented at the SLAC Summer Inst. on Particle Physics, 27 July- 7 August 1981; W. M. Geist, Talk presented at the Fourth Symposium on Elementary Particle Physics, Kazimierz, Poland, 25–30 May 1981, CERN/EP 81–79; K. P. Pretzl, Talk presented at the International Conference on High Energy Physics, Lisbon, 9–15 July 1981.
[42] C. Bromberg et al., preprint CALT-68-738 (1979).
[43] M. D. Corcoran et al., *Phys. Rev. Lett.* **41**, 9 (1979).
[44] C. Bromberg et al., *Phys. Rev. Lett.* **43**, 565 (1979).
[45] M. Dris et al., *Phys. Rev.* **D19**, 1361 (1979)